HAL
open science

Effects of the Electrolyte Concentration on the Nature of the Solid Electrolyte Interphase of a Lithium Metal Electrode

Justine Touja, Parnian Salembier Peyrovi, Yann Tison, Hervé Martinez, Olinda Gimello, Nicolas Louvain, Lorenzo Stievano, L. Monconduit

To cite this version:

Justine Touja, Parnian Salembier Peyrovi, Yann Tison, Hervé Martinez, Olinda Gimello, et al.. Effects of the Electrolyte Concentration on the Nature of the Solid Electrolyte Interphase of a Lithium Metal Electrode. Energy Technology, 2023, 11 (1), pp.2201037. 10.1002/ente.202201037 . hal-03884752

HAL Id: hal-03884752

https://univ-pau.hal.science/hal-03884752v1

Submitted on 28 Feb 2023

HAL is a multi-disciplinary open access archive for the deposit and dissemination of scientific research documents, whether they are published or not. The documents may come from teaching and research institutions in France or abroad, or from public or private research centers.

L'archive ouverte pluridisciplinaire **HAL**, est destinée au dépôt et à la diffusion de documents scientifiques de niveau recherche, publiés ou non, émanant des établissements d'enseignement et de recherche français ou étrangers, des laboratoires publics ou privés.

Check for updates

Energy Technology
Generation, Conversion, Storage, Distribution
www.entechnol.de

21944296, 2023, 1, Downloaded from https://onlinelibrary.wiley.com/doi/10.1002/ente.202201037 by Université De Pau Et Des Pays, Wiley Online Library on [28/02/2023]. See the Terms and Conditions (https://onlinelibrary.wiley.com/terms-and-conditions) on Wiley Online Library for rules of use; OA articles are governed by the applicable Creative Commons License

Effects of the Electrolyte Concentration on the Nature of the Solid Electrolyte Interphase of a Lithium Metal Electrode

Justine Touja, Parnian Salembier Peyrovi, Yann Tison, Hervé Martinez, Olinda Gimello, Nicolas Louvain, Lorenzo Stievano, and Laure Monconduit**

The need of more powerful systems with higher energy density raises a lot of interest in lithium metal batteries (LMBs). As LMBs suffer from safety concerns due to the dendrite growth, several strategies have been studied to limit this growth. Using a highly concentrated electrolyte allows a homogeneous lithium plating that delays the formation of dendrites. Herein, different techniques are used in order to better understand the beneficial role of the salt concentration in the lithium plating/stripping. Operando Fourier transform infrared spectroscopy highlights the better reversibility of the Li^+ solvation in the 5 M lithium bis(trifluoromethanesulfonyl) imide (LiTFSI) in 1,2-dioxolane/1,3-dimethoxyethane electrolyte in comparison with the 1 M electrolyte. This obviously leads to different electrolyte decompositions during the lithium plating/stripping and changes the nature of the electrode solid electrolyte interphase (SEI) depending on the salt concentration. Gas chromatography coupled with mass spectrometry as well as X-ray photoelectron spectroscopy confirms that with the 5 M LiTFSI electrolyte the salt is preferentially reduced during the plating/stripping, leading to a more inorganic SEI on the lithium metal electrode.

1. Introduction

The ever-increasing demand for batteries with higher energy density creates tension on the lithium-ion battery (LIB) market. Having LIBs likely reached their limits in terms of performance, the need of new battery systems with higher energy densities becomes urgent. In this regard, lithium metal is considered the best candidate as negative electrode due to its very low standard potential (−3.04 V vs SHE) and its high specific capacity (3860 mAh g^{-1}). The uneven deposition of lithium, however, leads to the formation of protrusions, called dendrites, on the lithium metal surface that can grow through the separator and create short-circuits or fire hazards. Moreover, some lithium is lost during each cycle due to the formation of "dead lithium," while the constant reaction between the electrolyte and the electrode leads to low coulombic efficiencies.

So far, some solutions have been proposed in the literature to protect lithium anodes, avoid dendrite growth, and improve the coulombic efficiency. Apart from lithium battery systems employing solid electrolytes,[1] different research strategies have been proposed to continue working with the more advantageous liquid electrolytes. For instance, it has been suggested to protect metallic lithium from dendrite growth and electrolyte decomposition by applying a coating layer. The latter can be produced using different techniques such as atomic layer deposition or chemical reaction between the electrode and a coating agent, either applied as a pretreatment or included in the electrolyte as an additive.[2–7] An alternative strategy largely discussed in the literature is the use of lithiophilic materials as hosts for lithium.[8–10] Using such materials could lead to the development of anode free batteries suppressing all previously mentioned lithium metal issues.[11,12] Working on the electrolyte formulation, on the other hand, seems so far the best strategy to improve battery safety. Indeed, Zhang et al. showed that adjusting the lithium salt concentration and introducing FEC as an additive in the electrolyte allow the formation of a stable solid electrolyte interphase (SEI) that favors a nondendritic lithium deposition over cycling.[13] The increase of salt concentration in the electrolyte tends to modify its properties as well as battery performance.

J. Touja, O. Gimello, N. Louvain, L. Stievano, L. Monconduit
CNRS
ENSCM
ICGM
Université Montpellier
34293 Montpellier, France
E-mail: Lorenzo.stievano@umontpellier.fr;
laure.monconduit@umontpellier.fr

J. Touja, H. Martinez, N. Louvain, L. Stievano, L. Monconduit
CNRS
Réseau sur le Stockage Electrochimique de l'Energie (RS2E)
80039 Amiens, France

P. Salembier Peyrovi, Y. Tison, H. Martinez
E2S UPPA
CNRS
IPREM
Université de Pau et des Pays de l'Adour
64053 Pau, France

The ORCID identification number(s) for the author(s) of this article can be found under https://doi.org/10.1002/ente.202201037.

© 2022 The Authors. Energy Technology published by Wiley-VCH GmbH. This is an open access article under the terms of the Creative Commons Attribution-NonCommercial License, which permits use, distribution and reproduction in any medium, provided the original work is properly cited and is not used for commercial purposes.

DOI: 10.1002/ente.202201037

For example, the flammability of carbonate liquid electrolytes has shown to be reduced just by increasing the lithium salt concentration from 1 to 4 M.[14] This effect can be attributed, in highly concentrated electrolytes, to the low amount of free solvent molecules, usually responsible of the electrolyte flammability, because many of them are engaged in Li^+ solvation.[15] For more than a decade, highly concentrated electrolytes have been proven to limit dendrite growth, and enhance coulombic efficiency and cycle life of lithium metal cells.[16] In 2013, Suo et al. proposed for the first time the concept of solvent-in-salt (SIS) electrolytes, in which both the weight and volume ratio of salt-to-solvent are higher than 1.[17] With a 7 M SIS electrolyte, they could mitigate the capacity fading of a Li–S battery. More recently, other research teams showed that increasing salt concentration in the electrolyte modifies the morphology of the deposited lithium, with a general decrease of dendritic lithium growth.[18,19] When a current density is applied to a cell, a concentration gradient appears, which is modified with the salt concentration in the electrolyte, and impacts the morphologies and the dendrite growth delay.[20]

Herein, we use different characterization techniques in order to better understand the beneficial influence of the high concentration electrolytes on lithium galvanostatic plating/stripping. Two concentrations of lithium bis(trifluoromethanesulfonyl) imide (LiTFSI) in 1,2-dioxolane (DOL)/1,3-dimethoxyethane (DME) were compared and will be referred as 1 M LiTFSI and 5 M LiTFSI. The Li^+ solvation/desolvation in a 5 M electrolyte was studied with operando Fourier transform infrared (FTIR) spectroscopy and compared to the solvation/desolvation occurring in a standard electrolyte (1 M). As the Li^+ solvation reversibility was different depending on the salt concentration, the electrolyte decomposition and the nature of the SEI created during the Li plating/stripping were studied with gas chromatography coupled with mass spectrometry (GC–MS) and X-ray photoelectron spectroscopy (XPS). These different techniques confirm that the nature of the SEI varies with the electrolyte concentration and suggest that the improved performance with a highly concentrated electrolyte is due to a more inorganic SEI due to the reaction between the electrode and the electrolyte salt.

2. Results and Discussion

The different electrolytes were first characterized by Raman and FTIR spectroscopy. **Figure 1**a shows the Raman spectra of 1 and 5 M LiTFSI-based electrolytes as well as that of the DOL/DME solvent mixture. New bands (e.g., at 740 and 747 cm^{-1}; cf., Figure 1b) appear in the spectra when the LiTFSI salt is added to the solvent mixture, their intensity increasing with the salt concentration. It is noteworthy that these bands are not upshifted as mentioned in a previous report.[19] These bands correspond to the stretching (ν) of the S—N and C—S bonds as well as the bending (δ) of the CF_3 groups of the TFSI anion.[21,22] The band at 746 cm^{-1}, which corresponds to the major contribution in the LiTFSI spectrum (cf., Figure S1, Supporting Information) and which increases with the salt concentration, can be attributed to the formation of contact ion pairs (CIP) or aggregates (AGG).[23] The stretching and rocking (ρ) vibrations of the C–O–C and CH_2 groups in glymes visible at 850 cm^{-1} for free DME molecules (Figure 1c), on the other hand, are shifted to 872 cm^{-1} when DME is solvating Li^+ ions (Li^+-DME).[22] The peaks in the Raman spectra were deconvoluted to quantify the amount of free TFSI anion, CIP or AGG, free DME, and coordinated DME (Figure S2, Supporting Information). For both electrolyte concentrations, the deconvolutions for the free DMEs compared to the coordinated DME molecules are difficult due to the weak intensity of the peaks. It can, however, clearly be concluded that there are more coordinated DMEs in the 5 M than in the 1 M LiTFSI-based electrolyte. For the free TFSI and CIP or AGG part, the results are much clearer, and conclusions can be

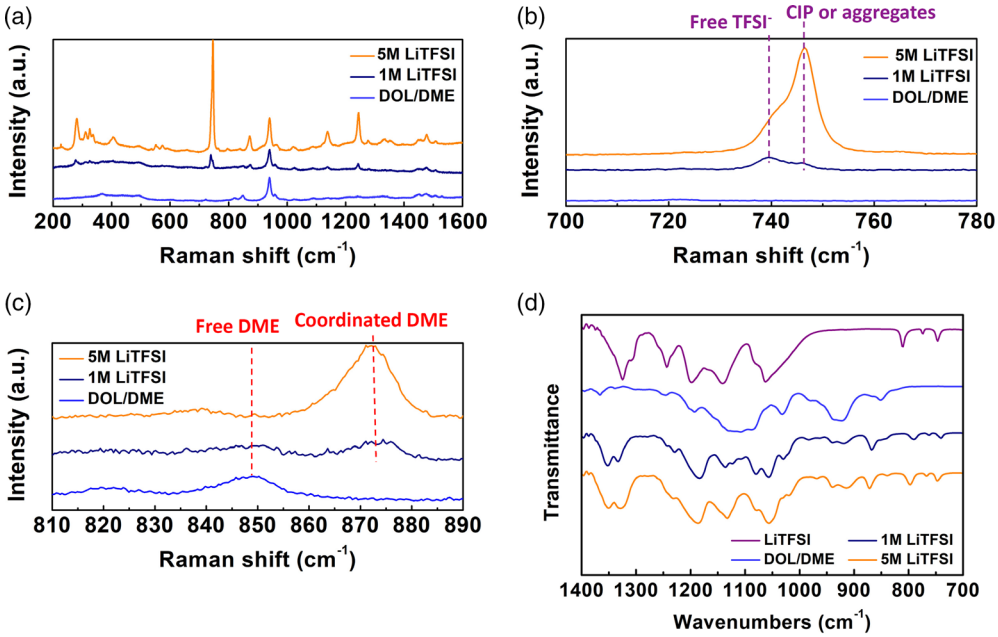

Figure 1. a–c) Raman spectra and d) FTIR spectra of the DOL/DME mixture with and without LiTFSI salt.

© 2022 The Authors. Energy Technology published by Wiley-VCH GmbH

21944296, 2023, 1, Downloaded from https://onlinelibrary.wiley.com/doi/10.1002/ente.202201037 by Université De Pau Et Des Pays, Wiley Online Library on [28/02/2023]. See the Terms and Conditions (https://onlinelibrary.wiley.com/terms-and-conditions) on Wiley Online Library for rules of use; OA articles are governed by the applicable Creative Commons License

drawn based on the peak areas, with 71% and 29% of free TFSI, and 29% and 71% of CIP or AGG for the 1 and 5 M LiTFSI-based electrolytes, respectively.

The FTIR spectra of the LiTFSI salt, the DOL/DME mixture, and the two electrolytes are shown in Figure 1d (Figure S5, Supporting Information). The LiTFSI salt shows a characteristic band at 1335 cm^{-1} whereas the 1 M and 5 M LiTFSI electrolytes show two bands at 1354 and 1335 cm^{-1}. As the latter grows with the salt concentration, it can be logically assigned to the presence of CIP or AGG, whereas the former can be attributed to the solvated TFSI anion. Another noteworthy band, at 850 cm^{-1}, corresponds to ν(COC) and $\rho(CH_2)$ of free DME. This band intensity decreases by increasing salt concentration, while simultaneously a new band at 868 cm^{-1} due to Li^+-DME grows. Unfortunately, the characteristic bands of DOL and LiTFSI fall at similar energies, which make it difficult to follow the influence of the concentration on Li^+ solvation with DOL.

In summary, the increase of salt concentration in the electrolyte leads to the formation of CIP and AGG, and thus to a modification of the ionic conductivity (see the impedance electrochemical impedance spectroscopy [EIS] measurements (Figure S3, Supporting Information) and the transference number (**Table 1**)). As previously reported in the literature for $LiPF_6$ in EC/DMC, an increase in salt concentration of the electrolyte corresponds to an increase of the conductivity up to a maximum, followed by a decrease when the concentration is further raised.[24] This can explain why the conductivity of the 5 M LiTFSI electrolyte is lower than the one of 1 M LiTFSI. It is worth mentioning that if the concentration of the salt in the electrolyte is too high, the conductivity might be too low hindering the cells to work. Moreover, the calculated transference number also decreases with increasing salt concentration, which is probably due to the formation of CIP leading to a slowing of the ions diffusion.[25] In addition, one should notice that, depending on the method used to measure the transference number, the results can be different, as shown with those calculated by Suo et al.[17] Moreover, even though the method used here is that developed by Bruce and Vincent, the results can be different because errors may subsist for the values of the resistance measured after the EIS experiments, and/or because the current measured during the chronoamperometry had not yet reached the steady state.[19] For these reasons, it is very difficult to provide a conclusive statement about this parameter.

The stability of the electrolytes and the influence of salt concentration on the possible corrosion of aluminum, usually employed as the current collector of positive electrodes in full cells, were studied by linear sweep voltammetry (LSV), with a lithium metal foil as the negative electrode and an aluminum foil as the positive electrode. With the 1 M LiTFSI electrolyte, the current density is stable up to 4.6 V, and then sharply increases (Figure S4, Supporting Information), which means that above this potential the electrolyte starts to corrode the aluminum or to decompose. The 5 M LiTFSI electrolyte, on the other hand, is stable up to 4.8 V. The coin cells were opened right after the LSV, in order to evaluate the corrosion of the aluminum electrodes. While some pits are visible on the surface of the aluminum foil with the 1 M LiTFSI electrolyte (Figure S4b, Supporting Information), none are observed on the aluminum used with the 5 M LiTFSI electrolyte (Figure S4c, Supporting Information). Increasing the concentration helps extending the potential window and avoiding the corrosion of the current collector at high potential. The current density increase that appears after 4.8 V for the highly concentrated electrolyte is then probably due to the oxidation of the TFSI anion.[26]

To verify the impact of the increase of salt concentration on lithium plating, galvanostatic plating/stripping measurements were carried out with symmetrical cells with a current density of 1 mA cm^{-2} and an areal capacity of 1 mAh cm^{-2} (**Figure 2**). The cell made with the high concentrated electrolyte presents a very stable polarization around 0.08 V for at least 250 h, whereas that measured with 1 M LiTFSI exhibits a chaotic variation of the potential after 20 h probably due to electrolyte degradation and/or dendrite formation (Figure 2a), as suggested for a similar behavior by previous studies.[27] More interestingly, although the overpotential is slightly higher (by ≈0.1 V) with a current density of 3 mA cm^{-2} (Figure 2b), the polarization of the symmetric cell with the 5 M LiTFSI electrolyte is quite stable for 200 h, whereas with the low concentration electrolyte the overpotential rapidly increases due to the continuous electrolyte decomposition.

EIS measurements were carried out in symmetric cells in order to follow the evolution of the resistance during the plating/stripping experiments. The Nyquist diagrams obtained under open-circuit voltage (OCV) conditions, shown in Figure 2c, indicate that the global impedance is higher with the 1 M LiTFSI electrolyte than with the 5 M one. The contact between the lithium metal electrode and the electrolyte creates a chemical SEI more resistive in the case of the low concentrated electrolyte. After five cycles, an important decrease of the impedance is observed for both electrolytes, which can be attributed to surface depassivation in the first plating/stripping cycles and the subsequent formation of a new SEI layer. Although the ionic resistances of the electrolytes, that correspond to the first semicircle intercept on Nyquist plots,[28,29] are very similar for both electrolytes (around 12 Ω) during OCV, the value increases during cycling with the 1 M one. This suggests that, during the plating/stripping cycles, some species are dissolved in the electrolyte leading to a variation of the concentration. In the case of 5 M LiTFSI, this resistance is the same even after 50 cycles, demonstrating the system stability during the experiment. Operando attenuated total reflection FTIR (ATR-FTIR) spectroscopy was applied during the plating/stripping experiment to get further insight on the evolution of the electrolytes in the working symmetric cells. In the first cycle, a passivation layer is created on the ATR crystal, which can induce an irreversible variation on the following spectra. For this reason, the reference spectrum allowing the calculation of the relative variation of the spectral intensity during the different processes was selected among those recorded during a 5 min OCV after the first full plating/stripping cycle. $\Delta R/R$ difference spectra highlighting the evolution of the intensity of different bands obtained after the second and third

Table 1. Electrolyte properties depending on the salt concentration.

Electrolytes	Conductivity [mS cm^{-1}]	Transference number of Li^+
LiTFSI (1 M) + DOL/DME	12	0.37
LiTFSI (5 M) + DOL/DME	3	0.18

© 2022 The Authors. Energy Technology published by Wiley-VCH GmbH

21944296, 2023, 1, Downloaded from https://onlinelibrary.wiley.com/doi/10.1002/ente.202201037 by Université De Pau Et Des Pays, Wiley Online Library on [28/02/2023]. See the Terms and Conditions (https://onlinelibrary.wiley.com/terms-and-conditions) on Wiley Online Library for rules of use; OA articles are governed by the applicable Creative Commons License

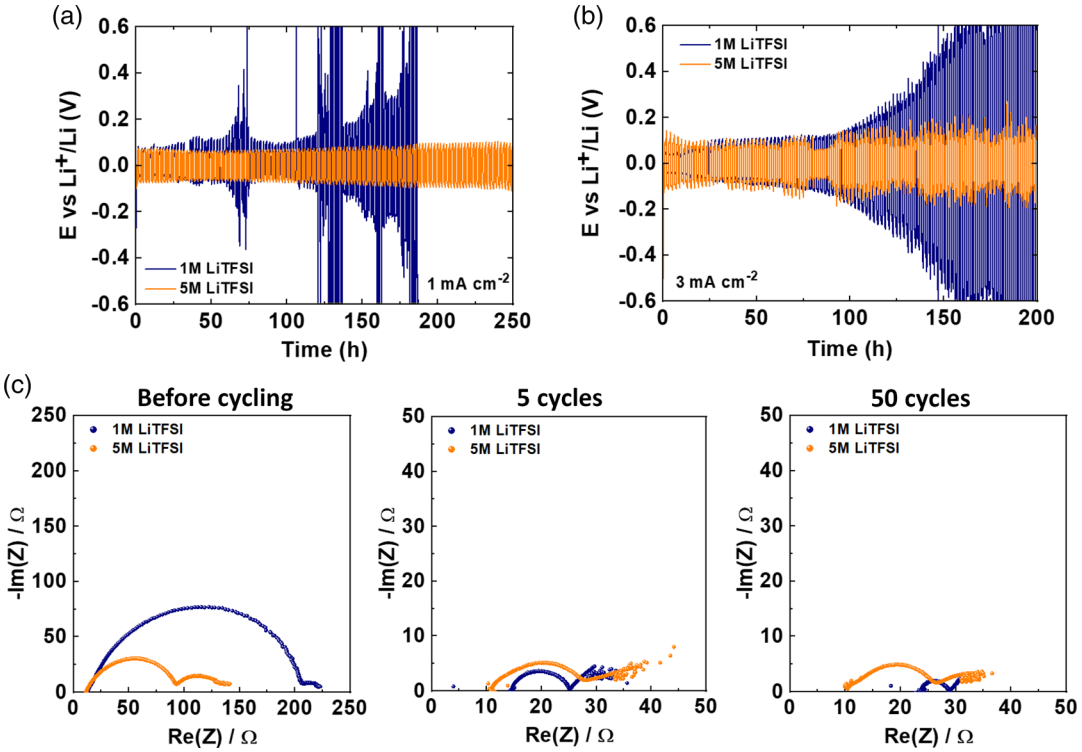

Figure 2. Li metal plating/stripping curves of Li|Li symmetric cells with 1 M LiTFSI and 5 M LiTFSI at a current density of a) 1 mA cm^{-2} and b) 3 mA cm^{-2}. c) Nyquist plots of the Li|Li cells with 1 M LiTFSI and 5 M LiTFSI before cycling, after 5 cycles, and after 50 cycles of plating/stripping at 1 mA cm^{-2}.

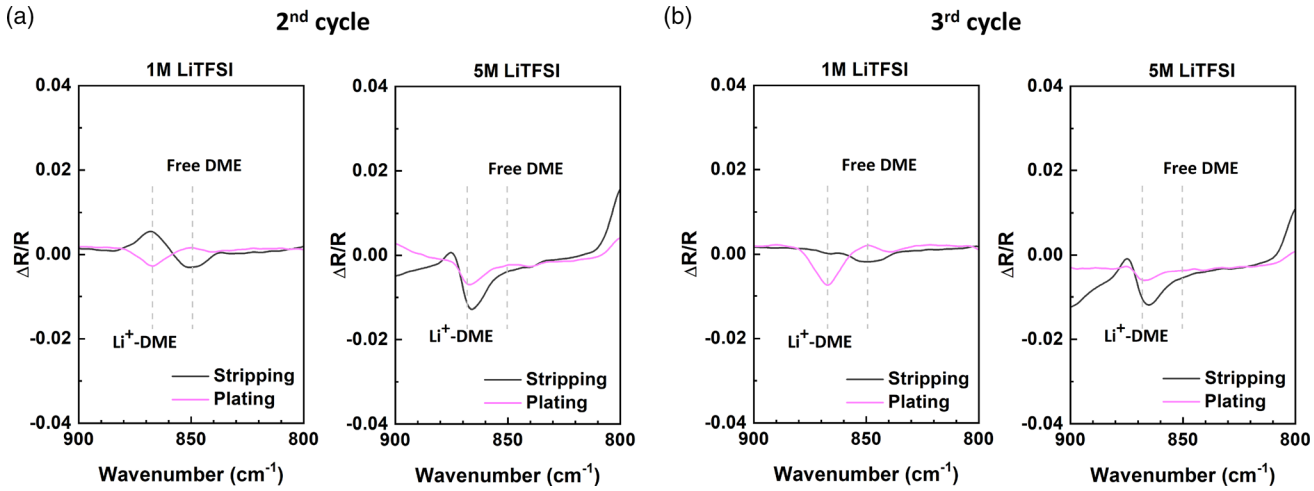

Figure 3. Operando ATR-FTIR difference spectra of 1 and 5 M LiTFSI electrolytes after the a) second cycle and the b) third cycle. The relative intensity is calculated with the last spectrum of the first cycle as reference.

cycles are shown in **Figure 3**. Positive and negative peaks indicate the increase and the decrease of the intensity of specific bands, respectively, which are connected to Li^+-DME and free DME species, during plating and stripping.

At the end of the second stripping with the 1 M LiTFSI electrolyte, the local increase of the concentration of solvated Li^+-DME species is well identified by the decrease and the increase in intensity of the characteristic bands of free DME and Li^+-DME, respectively (Figure 3a). The opposite result is obtained during the following stripping process, confirming the reproducibility of the local concentration of the different species and thus the reversibility of the ions solvation/desolvation mechanism. However, after the third cycle, the Li^+-DME band is not positive, suggesting a decrease of the amount of Li^+-DME solvated species during Li stripping (Figure 3b). This can be explained with the growth of the Li electrode thickness during cycling caused by the formation of dendrites, inactive lithium, and/or inactive electrolyte

© 2022 The Authors. Energy Technology published by Wiley-VCH GmbH

21944296, 2023, 1, Downloaded from https://onlinelibrary.wiley.com/doi/10.1002/ente.202201037 by Université De Pau Et Des Pays, Wiley Online Library on [28/02/2023]. See the Terms and Conditions (https://onlinelibrary.wiley.com/terms-and-conditions) on Wiley Online Library for rules of use; OA articles are governed by the applicable Creative Commons License

decomposition products. When this layer becomes too thick compared to the probed depth, the solvated Li^+-DME species are too far from the ATR crystal and cannot be detected anymore.

For the 5 M LiTFSI electrolyte, the results are, however, quite different. No variation in intensity is detected for the characteristic band of DME at 850 cm^{-1} during the polarization tests, which can be explained by the constant very low amount of free solvent molecules. Concerning the band representing Li^+-DME, its intensity does not simply vary with the concentration during stripping, as observed in the previous case: instead of a single positive one, a negative and a positive band positioned at lower and higher energies are observed (865 and 870 cm^{-1}, respectively), which can be explained by the blueshift of the signal of Li^+-DME solvated species. Indeed, the characteristic band of the solvated Li^+-DME undergoes a blueshift when the salt concentration increases (Figure S5, Supporting Information). Contrary to the low concentration electrolyte, no significant change is observed after the third cycle, suggesting a better reversibility of the solvation/desolvation process and thus a higher stability of the electrode with the high concentration electrolyte. The reversibility of Li^+ solvation, indeed, indirectly probes the evolution of the electrochemical mechanism near the electrode surface and thus of the SEI created during the galvanostatic measurements.[30] The differences observed with the FTIR spectroscopy for both electrolytes suggest that the salt concentration has an influence on the nature of the SEI created on the Li electrode surface during the measurement and then on the Li plating.

Concerning the nature of the SEI, GC–MS measurements were carried out to better understand the role of the solvent in the formation of the SEI. Indeed, these analyses reveal that, for both electrolytes, DOL seems to participate more than DME to the formation of the SEI (Figure S6, Supporting Information) because it decreases more rapidly than DME after OCV as well as after cycling. However, increasing the concentration decreases the percent of consumed DOL because only 50% is lost in 5 M LiTFSI against 70% in 1 M LiTFSI. This result suggests that the SEI formed with the high concentration electrolyte should be more inorganic than with 1 M LiTFSI resulting from the salt anion decomposition as shown in previous reports.[17,18,31,32]

In order to confirm this hypothesis, XPS analysis on Li electrode surfaces was carried out to identify the SEI nature as a function of the salt concentration, after 2 h of OCV as well as after 50 plating/stripping cycles. The XPS spectra recorded after 2 h of OCV are reported in Figure S7, Supporting Information. For both LITFSI concentrations, the C 1*s* spectra display three peaks at 285.0 eV (C–C/C–H), 286.5 eV (C–O), and 289.0 eV, which are associated with organic molecules. The peak at higher binding energy (291.0 eV) is associated with carbonate ions. The presence of a peak at low binding energy (283.5 eV) can be attributed to carbon in the vicinity of lithium (lithium carbide or carbon adsorbed on the surface of lithium). On the O1*s* spectra, two peaks are observed at 528.5 and 531.6 eV; they can, respectively, be assigned to the oxygen atoms of Li_2O and to oxygen atoms bound to carbon or to hydrogen (as in LiOH). Finally, the Li 1*s* peak is highly asymmetrical and can be fitted with two contributions: one at 53.8 eV, associated with the lithium atoms of Li_2O, and a second peak at 55.0 eV,

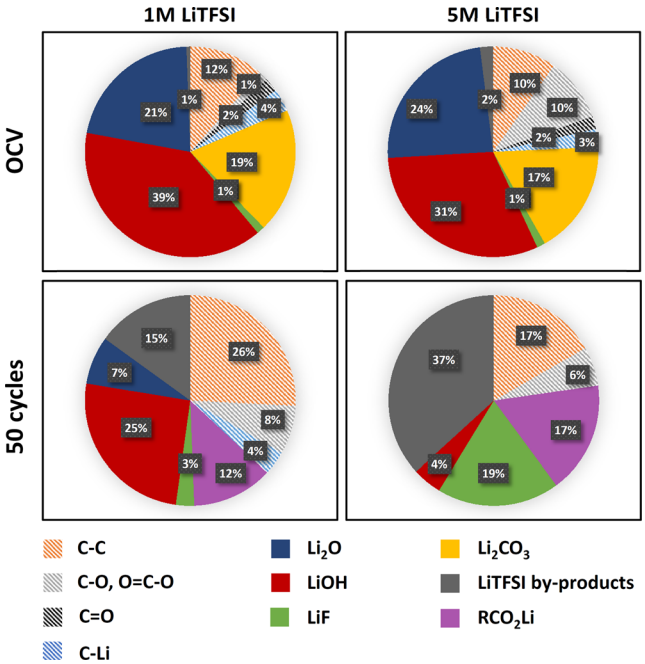

Figure 4. SEI composition as derived from XPS quantification of Li metal electrodes after OCV and after 50 cycles with 1 M LiTFSI and 5 M LiTFSI electrolytes. The striped and plain areas represent the inorganic and organic species, respectively.

correspond to LiOH or Li_2CO_3. We also observe, in weak intensities, the presence of the F 1*s* and the S 2*p* peaks (not shown). The chemical composition (in atomic percent) is reported in the top panels of **Figure 4**. It shows that the components of the chemical SEI created on the Li metal electrode during the OCV are the same with both electrolytes. This initial SEI is mostly constituted of inorganic lithiated species such as Li_2O, LiOH, Li_2CO_3 (75%–80%), together with organic species (20%–30%) identified by the C 1*s* peaks at 285.0, 286.5, and 289.0 eV.

After 50 cycles of plating/stripping, the F 1*s* and the S 2*p* core peaks are more intense and are presented in **Figure 5**, together with the C 1*s*, O 1*s*, and S 2*p* peaks. Regarding the sample cycled with the 1 M LiTFSI electrolyte, the C 1*s*, O 1*s*, and Li 1*s* core peaks are quite similar to those recorded after OCV, with two noteworthy differences: first, the C 1*s* carbonate peak at ≈291 eV is not present, and second, a small contribution associated with LiF is observed on the Li 1*s* spectrum at 56.3 eV. In the F 1*s* spectrum, the spectrum can be deconvoluted into two peaks corresponding to F–SO_2 species (688.8 eV) and LiF (685.3 eV). In the S 2*p* region, one can observe two doublets at 160.5–161.7 eV (Li_2S) and 167.0–168.2 eV (Li_2SO_4, F–SO_2). Hence, new species (LiF, Li_2S, Li_2SO_4) appear at the surface of the Li electrode, suggesting LiTFSI decomposition during the experiment.[33–35] For the sample cycled with the 5 M LiTFSI electrolyte, several significant differences compared to the results obtained after 2 h of OCV are observed: in the C 1*s* region, the two peaks of Li–C (283.5 eV) and Li_2CO_3 (291.0 eV) disappear, while a new peak, associated with C—F bonding, appears at 292.0 eV; the Li_2O peak in the O 1*s* region is absent; the LiF peak (56.0 eV) grows, while the Li_2O peak at 54.0 eV disappears. In the F 1*s* region, two peaks can be associated with Fluorine bound to

© 2022 The Authors. Energy Technology published by Wiley-VCH GmbH

21944296, 2023, 1, Downloaded from https://onlinelibrary.wiley.com/doi/10.1002/ente.202201037 by Université De Pau Et Des Pays, Wiley Online Library on [28/02/2023]. See the Terms and Conditions (https://onlinelibrary.wiley.com/terms-and-conditions) on Wiley Online Library for rules of use; OA articles are governed by the applicable Creative Commons License

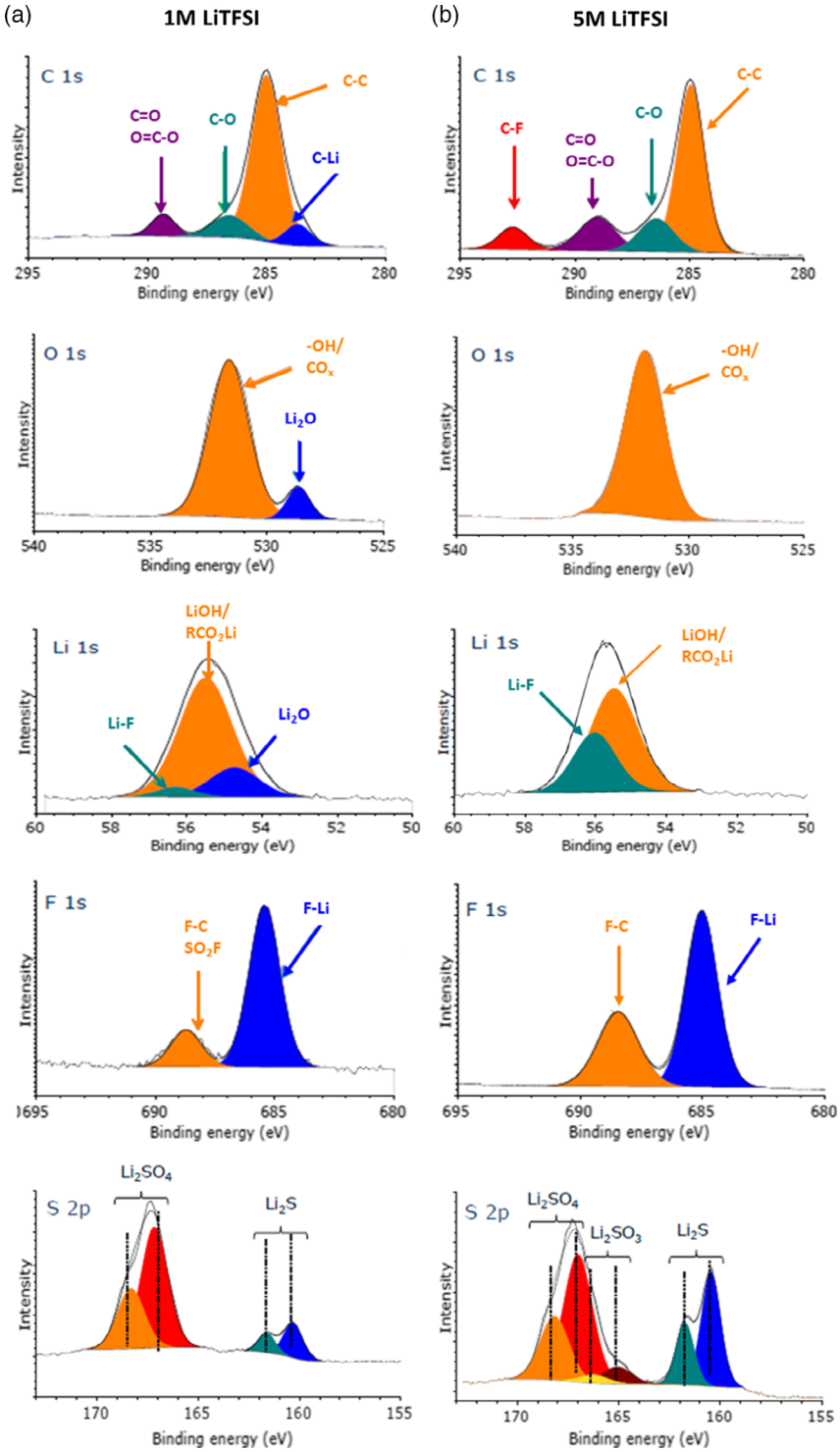

Figure 5. XPS spectra of Li electrodes after 50 plating/stripping cycles with a) 1 M LiTFSI and b) 5 M LiTFSI electrolytes.

carbon (688.3 eV) and LiF (685.0 eV). Finally, the S 2*p* core peaks are composed of three doublets at 160.5–161.7 eV (Li_2S), 165.1–166.7 eV (Li_2SO_3), and 167.0–168.2 eV (Li_2SO_4, F–SO_2). These results clearly show that the composition of the SEI is significantly different for the two concentrations: indeed, a higher concentration of LiTFSI in the electrolyte leads to an increase of the amount of LiTFSI decomposition compounds in the SEI. From the XPS quantification data, the content of each species (in at%) detected at the Li electrodes surface was determined (Figure 4, bottom panels).

© 2022 The Authors. Energy Technology published by Wiley-VCH GmbH

21944296, 2023, 1, Downloaded from https://onlinelibrary.wiley.com/doi/10.1002/ente.202201037 by Université De Pau Et Des Pays, Wiley Online Library on [28/02/2023]. See the Terms and Conditions (https://onlinelibrary.wiley.com/terms-and-conditions) on Wiley Online Library for rules of use; OA articles are governed by the applicable Creative Commons License

Regarding SEI composition, for the 1 M LiTFSI electrolyte, after 2 h under OCV conditions, organic species (C–C, C–Li, C–O, and other –CO containing species) represent 19 at% of the probed sample, the remainder being inorganic species (Li_2CO_3 and LiOH). No big difference is observed for the highly concentrated electrolyte, apart from a slight increase of the organic species (25 at%). After 50 cycles, however, while only 23 at% organic species (mainly C–C and –CO-containing species) are detected in the SEI with the 5 M LiTFSI electrolyte, their amount increases up to ≈40 at% with the 1 M LiTFSI electrolyte. This observation can be related to a more intense solvent degradation during the plating/stripping in the low concentration electrolyte system, in line with the higher fraction of decomposed DOL observed by GC–MS. The higher percentage of inorganic species, especially LiF and LiTFSI by-products, observed for the electrode cycled with the 5 M LiTFSI electrolyte can be explained by the lower amount of free solvent molecules in the high concentration electrolyte, which preserves them from decomposition. These results show that using a highly concentrated electrolyte induces the formation of a more inorganic SEI, which seems to be beneficial for lithium plating because the symmetric cell with 5 M LiTFSI electrolyte shows better cyclability and stability compared with the 1 M one.

Summarizing the outcomes of the different analyses, the increase in salt concentration in the electrolyte results in the formation of bulkier species (CIP and AGG) than in a conventional low-concentration electrolyte. These species are expected to slow down the diffusion of Li^+ ions in the electrolyte and create steeper gradients in the vicinity of the electrode surface during plating or stripping, thus leading to an increase of the polarization, as observed at the beginning of the plating process. In spite of this reduced mobility, the substantially higher Li^+ concentration in the electrolyte ensures that the concentration remains high enough close to the electrode surface (in the current ranges applied here), as testified by the results of the in situ ATR-IR analyses. An additional effect to explain the more regular plating behavior of the 5 M LiTFSI electrolyte is surely related to the nature of the SEI, which is more inorganic in nature when the salt concentration in the electrolyte is increased, as shown by XPS. Most probably, both the increase in Li^+ concentration near the electrode surface and the inorganic nature of the SEI improving Li^+ diffusion toward the lithium metal surface contribute to a more homogeneous plating and a reduction of dendrite growth.

3. Conclusions

Lithium ion solvation in a high concentration electrolyte appears very different from that in a standard electrolyte, leading to the formation of CIP and AGG species which favor the reduction of the TFSI anions during lithium plating. The nature of the SEI formed on the lithium electrode is then modified, becoming more inorganic with the 5 M LiTFSI electrolyte. Moreover, while the SEI seems to be stable with the high concentration electrolyte, its composition evolves in the cell with 1 M LiTFSI during the plating/stripping experiments. This can be explained with the partial dissolution of the SEI formed with the low concentration electrolyte, proving the poorer stability of this system. Finally, the inorganic nature of the SEI created with the high concentration electrolyte is beneficial for preventing or at least delaying dendrite growth during lithium plating.

4. Experimental Section

Materials: The lithium bis(trifluoromethanesulfonyl)imide salt (LiTFSI, purity 99.95 %, Sigma-Aldrich) as well as 1,2-dioxolane (DOL, anhydrous, 99.8%, Sigma-Aldrich), and 1,3-dimethoxyethane (DME, anhydrous, 99.5%, Sigma-Aldrich) were used as received without any purification. The electrolytes were prepared by dissolving the desired amount of salt in a 1:1 (v:v) mixture of DOL and DME, and stirring overnight in an argon-filled glove box (MBraun, $H_2O < 0.5$ ppm, $O_2 < 0.5$ ppm) until complete dissolution of the salt, corresponding to the formation of transparent solutions.

Characterizations: Raman spectra of the electrolytes were measured with a Horiba Jobin-Yvon LabRAM ARAMIS spectrometer with an excitation wavelength of 473 nm, using an airtight in situ cell to avoid any contamination from air moisture. Operando ATR-FTIR analyses were carried out with a specifically designed in situ cell allowing the recording of IR spectra during the electrochemical measurement.[36,37] The working lithium electrode was punched in the middle in order to avoid the direct contact with the ATR crystal probe, and measure the evolution of the electrolyte in the vicinity of the lithium metal surface without touching it. The spectra were recorded in the 700–1400 cm^{-1} range with a resolution of 1 cm^{-1}. A new spectrum was automatically recorded for 30 s at regular intervals of 5 min.

Optical microscopy images were acquired with a Bresser LCD microscope (40X) directly inside an Ar-filled glove box to prevent any sample decomposition. The evolution of the electrolytes was analyzed with a gas chromatograph coupled to a mass spectrometer (GC–MS). Electrolytes were collected from the Celgard separator after OCV or 50 cycles by immersing it in an acetonitrile solution and diluted in 3 mL of high purity acetonitrile to be analyzed by GC–MS with a Shimadzu GCMS QP-2010 Plus apparatus. A Supel-Q-Plot capillary column (30 m × 0.32 mm × 15 μm) silicon based with a divinylbenzene phase was used because it effectively resolves C1–C4 hydrocarbons species, among which outgassing that we expect to observe. The carrier gas (He) was set a linear velocity of 32 cm s^{-1}. The injector was set at 250 °C, with a split ratio of 60. The oven temperature program was set to an initial temperature of 45 °C, held for 5 min, and then it was increased to 250 °C at 10 °C min^{-1} for 5 min. The detector transfer line and source temperature were set at 200 °C. The MS stage was switched off between 10 and 13.5 min during the elution of very intense acetonitrile peak.

XPS measurements were performed on a Thermo K-alpha spectrometer with a hemispherical analyzer and a microfocused (400 μm diameter microspot) monochromated radiation (Al Kα, 1486.6 eV) operating at 72 W under a residual pressure of 1.10–9 mbar. The pass energy was set to 20 eV. Charge effects, currently important for hybrid sample, were compensated by the use of a dual-beam charge neutralization system (low energy electrons and Ar+ ions) which had the unique ability to provide consistent charge compensation. All spectra were energy calibrated by using the hydrocarbon peak at a binding energy of 285.0 eV. Spectra were mathematically fitted with Casa XPS software using a least squares algorithm and a nonlinear Shirley-type background. The fitting peaks of the experimental curves were defined by a combination of Gaussian (70%) and Lorentzian (30%) distributions. Quantification was performed on the basis of Scofield's relative sensitivity factors.

Electrochemical Experiments: CR2032-type coin cells were assembled in an Ar-filled glove box, using Li electrodes punched out of a lithium metal ribbon (Sigma-Aldrich) both as reference and counter-electrode. For LSV measurements, the working electrode was a foil of aluminum whereas Li metal was used for the Li | Li symmetric cells. In all cases, the electrodes, with a diameter of 1.27 cm, were separated with a trilayer polyprolpylene polyethylene membrane (Celgard 2325) soaked with 100 μL of electrolyte. A MPG2 (Biologic) multichannel potentiostat was used for LSV and Li

© 2022 The Authors. Energy Technology published by Wiley-VCH GmbH

21944296, 2023, 1, Downloaded from https://onlinelibrary.wiley.com/doi/10.1002/ente.202201037 by Université De Pau Et Des Pays, Wiley Online Library on [28/02/2023]. See the Terms and Conditions (https://onlinelibrary.wiley.com/terms-and-conditions) on Wiley Online Library for rules of use; OA articles are governed by the applicable Creative Commons License

plating/stripping EIS measurements of the Li | Li cells were performed with a VSP (Biologic) potentiostat between 1 MHz and 10 mHz with an amplitude of 10 mV. The same EIS parameters were used to measure the ionic conductivity and the transference number of the electrolytes (cf., SI1 for more details).

Supporting Information

Supporting Information is available from the Wiley Online Library or from the author.

Acknowledgements

The authors thank the analysis and characterization platform from the "Pôle Chimie Balard" for granting access to Raman spectroscopy. The authors thank also the RS2E Network, the French National Research Agency (STORE-EX Labex Project ANR-10-LABX-76-01).

Conflict of Interest

The authors declare no conflict of interest.

Author Contributions

J.T.: electrodes preparation, electrochemical measurements, IES, IR ATR; P.S.P.: XPS measurements; Y.T.: XPS analysis; H.M.: XPS analysis supervising; O.G.: GCMS measurements; N.L.: IR ATR and impedance measurement and analysis; L.S.: spectroscopy and electrochemical measurements supervising; L.M.: electrochemical mechanism understanding and supervising of the whole study.

Data Availability Statement

The data that support the findings of this study are available from the corresponding author upon reasonable request.

Keywords

electrolytes, lithium anodes, lithium batteries, metal anodes, solid electrolyte interphase

Received: September 6, 2022
Revised: November 8, 2022
Published online: November 27, 2022

[1] K. Yoon, S. Lee, K. Oh, K. Kang, *Adv. Mater.* **2022**, *34*, 2104666.
[2] B. Yan, X. Li, Z. Bai, X. Song, D. Xiong, M. Zhao, D. Li, S. Lu, *J. Power Sources* **2017**, *338*, 34.
[3] S. Li, Q. Liu, X. Wang, Q. Wu, L. Fan, W. Zhang, Z. Shen, L. Wang, M. Ling, Y. Lu, *ACS Mater. Lett.* **2020**, *2*, 1.
[4] Y. Liu, D. Lin, P. Y. Yuen, K. Liu, J. Xie, R. H. Dauskardt, Y. Cui, *Adv. Mater.* **2017**, *29*, 1605531.
[5] X. Liang, Q. Pang, I. R. Kochetkov, M. S. Sempere, H. Huang, X. Sun, L. F. Nazar, *Nat. Energy* **2017**, *2*, 17119.
[6] Z. Tu, S. Choudhury, M. J. Zachman, S. Wei, K. Zhang, L. F. Kourkoutis, L. A. Archer, *Nat. Energy* **2018**, *3*, 310.
[7] J. Touja, N. Louvain, L. Stievano, L. Monconduit, R. Berthelot, *Batteries Supercaps* **2021**, *4*, 1252.
[8] D. Lin, Y. Liu, Z. Liang, H. W. Lee, J. Sun, H. Wang, K. Yan, J. Xie, Y. Cui, *Nat. Nanotechnol.* **2016**, *11*, 626.
[9] X. B. Cheng, T. Z. Hou, R. Zhang, H. J. Peng, C. Z. Zhao, J. Q. Huang, Q. Zhang, *Adv. Mater.* **2016**, *28*, 2888.
[10] P. Shi, X. Zhang, X. Shen, R. Zhang, H. Liu, Q. Zhang, *Adv. Mater. Technol.* **2020**, *5*, 1900806.
[11] Z. Xie, Z. Wu, X. An, X. Yue, J. Wang, A. Abudula, G. Guan, *Energy Storage Mater.* **2020**, *32*, 386.
[12] S. Nanda, A. Gupta, A. Manthiram, *Adv. Energy Mater.* **2021**, *11*, 2000804.
[13] K. Zhang, Y. An, C. Wei, Y. Qian, Y. Zhang, J. Feng, *ACS Appl. Mater. Interfaces* **2021**, *13*, 50869.
[14] S.-J. Cho, D.-E. Yu, T. P. Pollard, H. Moon, M. Jang, O. Borodin, S.-Y. Lee, *iScience* **2020**, *23*, 100844.
[15] H. Liang, X. Zuo, L. Zhang, W. Huang, Q. Chen, T. Zhu, J. Liu, J. Nan, *J. Electrochem. Soc.* **2020**, *167*, 090520.
[16] S. K. Jeong, H. Y. Seo, D. H. Kim, H. K. Han, J. G. Kim, Y. B. Lee, Y. Iriyama, T. Abe, Z. Ogumi, *Electrochem. Commun.* **2008**, *10*, 635.
[17] L. Suo, Y. S. Hu, H. Li, M. Armand, L. Chen, *Nat. Commun.* **2013**, *4*, 1481.
[18] J. Qian, W. A. Henderson, W. Xu, P. Bhattacharya, M. Engelhard, O. Borodin, J. G. Zhang, *Nat. Commun.* **2015**, *6*, 6362.
[19] S. Wang, J. Qu, F. Wu, K. Yan, C. Zhang, *ACS Appl. Mater. Interfaces* **2020**, *12*, 8366.
[20] P. Bai, J. Li, F. R. Brushett, M. Z. Bazant, *Energy Environ. Sci.* **2016**, *9*, 3221.
[21] I. Rey, P. Johansson, J. Lindgren, J. C. Lassègues, J. Grondin, L. Servant, *J. Phys. Chem. A* **1998**, *102*, 3249.
[22] D. Brouillette, D. E. Irish, N. J. Taylor, G. Perron, M. Odziemkowski, J. E. Desnoyers, *Phys. Chem. Chem. Phys.* **2002**, *4*, 6063.
[23] Y. Yamada, A. Yamada, *J. Electrochem. Soc.* **2015**, *162*, A2406.
[24] C. L. Berhaut, D. Lemordant, P. Porion, L. Timperman, G. Schmidt, M. Anouti, *RSC Adv.* **2019**, *9*, 4599.
[25] J. Zhao, L. Wang, X. He, C. Wan, C. Jiang, *J. Electrochem. Soc.* **2008**, *155*, A292.
[26] D. W. McOwen, D. M. Seo, O. Borodin, J. Vatamanu, P. D. Boyle, W. A. Henderson, *Energy Environ. Sci.* **2014**, *7*, 416.
[27] K. N. Wood, M. Noked, N. P. Dasgupta, *ACS Energy Lett.* **2017**, *2*, 664.
[28] E. Barsoukov, J. R. Macdonald, *Impedance Spectroscopy, Theory Experiment and Applications*, John Wiley & Sons, New York, NY **2005**.
[29] Y. D. Ko, J. G. Kang, J. G. Park, D. W. Kim, *J. Appl. Electrochem.* **2010**, *40*, 109.
[30] P. N. Le Pham, V. Gabaudan, A. Boulaoued, G. Åvall, F. Salles, P. Johansson, L. Monconduit, L. Stievano, *Energy Storage Mater.* **2022**, *45*, 291.
[31] S. Chen, J. Zheng, D. Mei, K. S. Han, M. H. Engelhard, W. Zhao, W. Xu, J. Liu, J.-G. Zhang, *Adv. Mater.* **2018**, *30*, 1706102.
[32] Y. Yamada, J. Wang, S. Ko, E. Watanabe, A. Yamada, *Nat. Energy* **2019**, *4*, 269.
[33] D. Aurbach, I. Weissman, A. Schechter, H. Cohen, *Langmuir* **1996**, *12*, 3991.
[34] C. Xu, B. Sun, T. Gustafsson, K. Edström, D. Brandell, M. Hahlin, *J. Mater. Chem. A* **2014**, *2*, 7256.
[35] G. G. Eshetu, X. Judez, C. Li, M. Martinez-Ibañez, I. Gracia, O. Bondarchuk, J. Carrasco, L. M. Rodriguez-Martinez, H. Zhang, M. Armand, *J. Am. Chem. Soc.* **2018**, *140*, 9921.
[36] A. Mullaliu, M. T. Sougrati, N. Louvain, G. Aquilanti, M.-L. Doublet, L. Stievano, M. Giorgetti, *Electrochim. Acta* **2017**, *257*, 364.
[37] C. Marino, A. Boulaoued, J. Fullenwarth, D. Maurin, N. Louvain, J.-L. Bantignies, L. Stievano, L. Monconduit, *J. Phys. Chem. C* **2017**, *121*, 26598.

© 2022 The Authors. Energy Technology published by Wiley-VCH GmbH

21944296, 2023, 1, Downloaded from https://onlinelibrary.wiley.com/doi/10.1002/ente.202201037 by Université De Pau Et Des Pays, Wiley Online Library on [28/02/2023]. See the Terms and Conditions (https://onlinelibrary.wiley.com/terms-and-conditions) on Wiley Online Library for rules of use; OA articles are governed by the applicable Creative Commons License